Astronomy & Astrophysics

Chandra observation of the dipping source XB 1254–690

R. Iaria, T. Di Salvo, G. Lavagetto, A. D' Aí, and N. R. Robba

Dipartimento di Scienze Fisiche ed Astronomiche, Università di Palermo, via Archirafi 36, 90123 Palermo, Italy
e-mail: iaria@fisica.unipa.it

ABSTRACT

We present the results of a 53 ks long Chandra observation of the dipping source XB 1254–690. During the observation neither bursts or dips were observed. From the zero-order image we estimated the precise X-ray coordinates of the source with a 90% uncertainty of 0.6″. Since the lightcurve did not show any significant variability, we extracted the spectrum corresponding to the whole observation. We confirmed the presence of the Fe XXVI K_α absorption lines with a larger accuracy with respect to the previous XMM EPIC pn observation. Assuming that the line width were due to a bulk motion or a turbulence associated to the coronal activity, we estimate that the lines were produced in a photoionized absorber between the coronal radius and the outer edge of the accretion disk.

Key words. accretion, accretion disks – stars: individual: XB 1254–690 – stars: neutron – X-rays: stars – X-rays: binaries – line: identification

1. Introduction

About 10 Low Mass X-ray Binaries (LMXB) are known to show periodic dips in their X-ray light curves and most of them also show X-ray burst activity. The dip intensities, lengths and shapes change from source to source, and, for the same source, from cycle to cycle. Among the dipping sources, XB 1254–690 (4U 1254–69), that also shows type-I X-ray bursts, is peculiar because it showed a cessation of its regular dipping activity (Smale & Wachter 1999). This source was observed for the first time by HEAO 1 A2 instrument (Mason et al. 1980) when an optical burst of ~20 s duration occurred. The optical counterpart to XB 1254–690, GR Mus, was identified by Griffiths et al. (1978) to be a faint blue object ($V = 19.1$), implying a ratio of X-ray to optical luminosity $L_x/L_{opt} \sim 200$, similar to those of other compact X-ray binaries with Population II companions (Lewin & Joss 1983).

EXOSAT observations showed the presence of type-I X-ray bursts and led to the discovery of recurrent X-ray dips with a period of 3.88 ± 0.15 h (Courvoisier et al. 1984, 1986). The duration of the dips was 0.8 h, representing 20% of the binary cycle, with a reduction of the X-ray flux between 20% and 90%. During the dips, X-ray variabilities were present on time scales 1–300 s. This complex time structure indicates that the obscuring region was clumpy and of variable size. A modulation with the same period of the X-ray dips was also observed in optical light curves, with the optical minimum occurring 0.2 cycles after the X-ray dip (Motch et al. 1987). The presence of dips and the lack of eclipse of the X-ray source gave a constraint on the inclination angle of the source that is between 65° and 73° (Courvoisier et al. 1986; Motch et al. 1987). X-ray bursts and X-ray dips were also present in a Ginga observation performed on August 1990 (Uno et al. 1997). On the other hand the dips were not present in a RXTE observation in 1997 between April 28 and May 1 (Smale & Wachter 1999). The cessation of the dipping activity indicated that the angular size of the disk edge (at the impact point with the accretion stream) decreased from 17°–25° to less than 10°, moreover there was no evidence of a simultaneous variation of the accretion rate or the location of the outer rim of the accretion disk (Smale & Wachter 1999). The dips were also absent during a BeppoSAX observation in 1998 (Iaria et al. 2001), appeared by the time of a RXTE observation in 2001 May, but were again not present in 2001 December (Smale et al. 2002).

Iaria et al. (2001) fitted the 0.1–100 keV BeppoSAX spectrum of XB 1254–690 adopting a multicolor disk-blackbody with an inner temperature of 0.85 keV plus a Comptonized component with an electron temperature of 2 keV and an optical depth of 19. The authors detected a hard excess at around 20 keV which might be accounted for adding a bremsstrahlung model with a temperature of 20 keV. Finally, there was also evidence in the BeppoSAX observation for an absorption edge at 1.27 keV with an optical depth of 0.15. Iaria et al. (2001) proposed that the Comptonized component could originate in a spherical cloud, or boundary layer, surrounding the neutron star while the bremsstrahlung component probably originates in an extended accretion disk corona with a radius of 10^{10} cm and a mean electron density of 1.7×10^{14} cm^{-3}.

Boirin & Parmar (2003) studied XB 1254–690 using two XMM-Newton EPIC pn observations in timing and small window mode with an exposure time of 10 and 13 ks, respectively. The continuum of the persistent emission in the 0.6–10 keV EPIC pn spectrum was fitted using a multicolor disk-blackbody, with an inner temperature between 2 and 2.3 keV, plus a power-law component with a photon index between 2.2 and 2.3. Furthermore Boirin & Parmar (2003) detected a Fe XXVI K_α and a Fe XXVI K_β absorption line centered at 6.96 and 8.16 keV, with upper limits on the line widths between 95 and 120 eV, and between 80 and 170 eV, respectively; finally they observed a soft excess around 1 keV that was modeled by a Gaussian emission line centered at 0.93 keV, with a line width of 175 eV and an equivalent width of ~30 eV.

Diaz Trigo et al. (2005) modeled the changes in both the X-ray continuum and the Fe absorption features during dipping of six bright LMXBs observed by XMM-Newton, included XB 1254–690. They concluded that the dips were produced by an increase in the column density and a decrease in the ionization state of the highly ionized absorber. Moreover, outside of the dips, the absorption line properties did not vary strongly with orbital phase, this implied that the ionized plasma had a cylindrical geometry with a maximum column density close to the plane of the accretion disk. Since dipping sources are normal LMXBs viewed from close to the orbital plane this implied that ionized plasmas are a common feature of LMXBs. In particular, Diaz Trigo et al. (2005) included absorption from a photoionized plasma (xabs in SPEX) in the spectral model to account for the narrow features near 7 keV. Reanalysing the XMM data of XB 1254–690 described above the authors obtained a ionization parameter associated to the persistent emission of $\log(\xi) = 4.3 \pm 0.1$ erg cm^{-2} s^{-1}.

Finally we note that the improved sensitivity and spectral resolution of Chandra and XMM-Newton are allowing to observe narrow absorption features, from highly ionized ions (H-like and He-like), in a larger and larger number of X-ray binaries. These features were detected from the micro-quasars GRO J1655–40 (Ueda et al. 1998; Yamaoka et al. 2001) and GRS 1915+105 (Kotani et al. 2000; Lee et al. 2002). Recently the Chandra High-Energy Transmission Grating Spectrometer (HETGS) observations of the black hole candidate H 1743–322 (Miller et al. 2004) have revealed the presence of blue-shifted Fe XXV and Fe XXVI absorption features suggesting the presence of a highly-ionized outflow. All LMXBs that exhibit narrow X-ray absorption features are all known dipping sources (see Table 5 of Boirin et al. 2004) except for GX 13+1. This source shows deep blue-shifted Fe absorption features in its HETGS spectrum, again indicative of outflowing material (Ueda et al. 2004). We conclude this brief resume observing that a recent Chandra spectral analysis of the dipping source XB 1916–053 showed the presence of several absorption features associated to Ne X, Mg XII, Si XIV and S XVI, Fe XXV and Fe XXVI (see Iaria et al. 2006; Juett & Chakrabarty 2006).

In this work we present a Chandra spectral analysis of the persistent emission from the dipping source XB 1254–690 in the 0.7–10 keV energy range using a long 53 ks Chandra observation. The observation covered around 3.8 orbital periods and the lightcurve showed no dips at all. We detected a Fe XXVI K$_\alpha$ absorption line, already observed with the XMM observation; the better energy resolution of Chandra and the larger statistics allowed to well determine its width. We discuss that the Fe XXVI absorption line was produced in a photoionized absorber placed between the coronal radius and the outer edge of the accretion disk.

2. Observation

XB 1254–690 was observed with the Chandra observatory on 2003 October 10 from 01:58:44 to 17:15:55 UT using the HETGS. The observation (Obsid 3823 in the Public Data Chandra Archive) had a total integration time of 53 ks, and was performed in timed graded mode. The HETGS consists of two types of transmission gratings, the Medium Energy Grating (MEG) and the High Energy Grating (HEG). The HETGS affords high-resolution spectroscopy from 1.2 to 31 Å (0.4–10 keV) with a peak spectral resolution of $\lambda/\Delta\lambda \sim 1000$ at 12 Å for HEG first order. The dispersed spectra were recorded with an array of six charge-coupled devices (CCDs) which are part of the Advanced CCD Imaging Spectrometer-S (Garmire et al. 2003)[1]. We processed the event list using available software (FTOOLS v6.0.2 and CIAO v3.2 packages) and computed aspect-corrected exposure maps for each spectrum, allowing us to correct for effects from the effective area of the CCD spectrometer.

The brightness of the source required additional efforts to mitigate "photon pileup" effects. A 512 row "subarray" (with the first row = 1) was applied during the observation reducing the CCD frame time to 1.74 s. Pileup distorts the count spectrum because detected events overlap and their deposited charges are collected into single, apparently more energetic, events. Moreover, many events ($\sim$90%) are lost as the grades of the piled up events overlap those of highly energetic background particles and are thus rejected by the on board software. We, therefore, ignored the zeroth-order events in our spectral analysis. On the other hand, the grating spectra were not, or only moderately (less than 10%), affected by pileup. In this work we analysed the 1st-order HEG and MEG spectra; since a 512 row subarray was applied the 1st-order HEG and MEG energy range were shrinked to 0.9–10 keV and 0.7–7 keV, respectively.

To determine the zero-point position in the image as precisely as possible, we estimated the mean crossing point of the zeroth-order readout trace and the tracks of the dispersed HEG and MEG arms. We obtained the following coordinates: RA = 12^{h}57^{m}37^s.153, Dec = −69°17′18″.98 (J2000.0, with a 90% uncertainty circle of the absolute position of 0.6″[2]). We compared the coordinates of XB 1254–690 obtained by us to the coordinates of the source reported by the the NASA HEASARCH tool "Coordinate Converter"[3]. The coordinates obtained with the tool were RA = 12^{h}57^{m}37^s.20, Dec = −69°17′21″.0 (referred to J2000.0), having an angular separation from the Chandra coordinates of 2″. We noted that Boirin & Parmar (2003) could not estimate more precise values of the coordinates because the spatial resolution of all the XMM-Newton EPIC cameras is larger than 2″. In Fig. 1 we reported the region of sky around the Chandra zero-order image of XB 1254–690.

In Fig. 2 we showed the 80 s bin time lightcurve taking into account only the events in the positive first-order HEG. The mean count rate in the persistent state was 2.8 count s^{-1}. During the observation neither bursts or dips were observed.
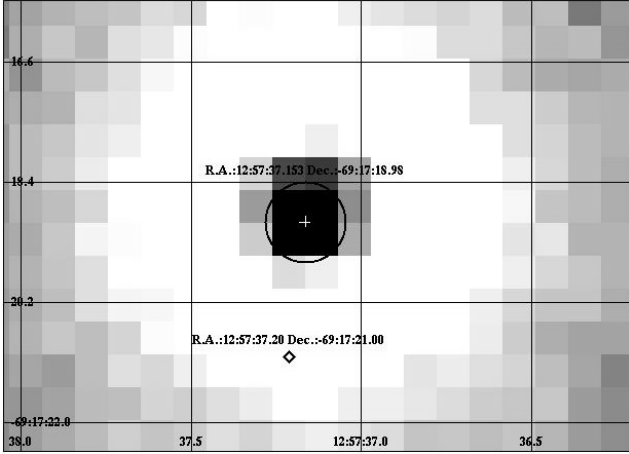
3. Spectral analysis

Because the lightcurve and the hardness ratio of the source did not show changes during the whole observation we selected the 1st-order spectra from the HETGS data along the entire observation with a total exposure time of 52 ks. Data were extracted from regions around the grating arms; to avoid overlapping between HEG and MEG data, we used a region size of 25 and 33 pixels for the HEG and MEG, respectively, along the cross-dispersion direction. The background spectra were computed, as usual, by extracting data above and below the dispersed flux. The contribution from the background is 0.4% of the total count rate. We used the standard CIAO tools to create detector response files (Davis 2001) for the HEG -1 (MEG -1) and HEG +1 (MEG +1) order (background-subtracted) spectra. After

---

[1] See http://asc.harvard.edu/cdo/about_chandra for more details.

[2] See http://cxc.harvard.edu/cal/ASPECT/celmon/ for more details.

[3] See http://heasarch.gsfc.nasa.gov/cgi-bin/Tools/convcoord/convcoord.pl

Fig. 1. Region of sky around the Chandra zero-order image of XB 1254–690. The coordinate system is referred to J2000. The black circle centered to the best estimation (white cross point) of the Chandra position has a radius of 0.6″. The diamond point indicates the position of XB 1254–690 (J2000) reported by the Heasarch "Coordinate Converter" tool (see text). The angular separation between the two points is 2″.
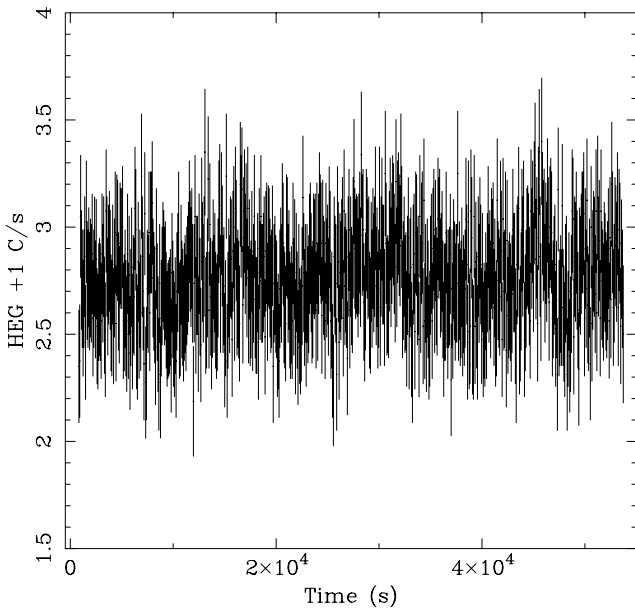
Fig. 2. The 53 ks lightcurve of XB 1254–690. During the observation neither bursts or dips were observed. The used events corresponds to the positive first-order HEG. The bin time is 80 s.

verifying that the negative and positive orders were compatible with each other in the whole energy range we coadded them using the script *add_grating_spectra* in the CIAO software, obtaining the 1st-order MEG spectrum and the 1st-order HEG spectrum. Finally we rebinned the resulting 1st-order MEG and 1st-order HEG spectra to 0.015 Å and 0.0075 Å, respectively.

To fit the continuum we used the rebinned spectra in the 0.7–7 keV and 0.9–10 keV for first-order MEG and first-order HEG, respectively. Initially we tried to fit the continuum using a single component and adding a systematic edge at around 2.07 keV with a negative optical depth of ~-0.2 to take in account of an instrumental artifact (see Miller et al. 2002, and references therein). Models composed of an absorbed power-law or an absorbed multicolor disk (MCD; Mitsuda et al. 1984)

gave χ^2(d.o.f.) of 3483(2725) and 2733(2725), respectively, and the data showed large residuals along the whole used energy range indicating a bad choice of the continuum. Following we tried models composed of two absorbed components finding three statistically equivalent models giving good fits, the first composed of a power law plus a MCD component as adopted by Boirin & Parmar (2003), the second composed of a MCD component plus a Comptonized component (CompST in XSPEC) as adopted by Iaria et al. (2001), and the third composed of a blackbody plus a power law with cutoff as reported by Smale et al. (2002); we obtained a χ^2(d.o.f.) of 2406(2723), 2447(2722), and 2412(2723), respectively.

From the fit of the model composed of a MCD plus a power law component we found an absorbing equivalent hydrogen column of $N_H = 0.24 \times 10^{22}$ cm^{-2}, a photon index of 2.3, a power-law normalization of 0.07, a temperature of the MCD component of 2.47 keV, a normalization associated to the MCD of 1.39, and an unabsorbed luminosity, assuming a distance to the source of 10 kpc (Courvoisier et al. 1986; hereafter we assume this value of distance to the source), of $\sim 1.2 \times 10^{37}$ erg s^{-1} in the 0.6–10 keV energy range. The best-fit values and the unabsorbed luminosity were comparable to those obtained by Boirin & Parmar (2003), indicating that the source was in a similar spectral state during this observation and the previous XMM observations. To confirm this result we analysed the RXTE ASM lightcurve of XB 1254–690. We observed that during the two XMM observations the ASM count rate was 2.24 ± 0.16 and 2.02 ± 0.26 C/s, while during this observation the ASM count rate was 2.66 ± 0.30 C/s with a similar intensity of the source as obtained from the spectral analysis.

From the fit of the model composed of a MCD plus a Comptonized component (CompST in XSPEC) we found an absorbing equivalent hydrogen column of $N_H \simeq 0.20 \times 10^{22}$ cm^{-2}, an electron temperature kT_e of 1.76 keV, an optical depth τ associated to the Comptonizing region of 25, and a normalization N_{compST} of 0.10. We fixed the internal temperature of the accretion disk kT_{in} to 0.855 keV as reported by Iaria et al. (2001) finding a MCD normalization k of 12.2. We found an unabsorbed luminosity of $\sim 1.2 \times 10^{37}$ erg s^{-1} in the 0.6–10 keV energy, compatible to that obtained by Iaria et al. (2001) in the same energy range. This was also confirmed looking at the ASM lightcurve of XB 1254–690, during the BeppoSAX observation the ASM count rate was 1.96 ± 0.60 C/s (see Fig. 4). Iaria et al. (2001) detected an absorption edge at 1.276 in the BeppoSAX spectrum, we added this component fixing the energy threshold and finding a corresponding optical depth <0.014, not compatible to that previously detected of 0.154 ± 0.059.

From the fit of the model composed of a blackbody plus a power law with cutoff we found an absorbing equivalent hydrogen column of $N_H \simeq 0.18 \times 10^{22}$ cm^{-2}, a blackbody temperature kT_{BB} of 1.47 keV, and a blackbody normalization N_{BB} of 2.3 $\times 10^{-3}$. We fixed the energy cutoff of the power law to 5.9 keV, as reported by Smale et al. (2002) for the persistent emission of XB 1254–690, finding a photon index of 1.03 and a power-law normalization of 0.145. All the best-fit values are compatible to those obtained by Smale et al. (2002) except N_{BB} that was slightly lower indicating a lower emission of blackbody during the Chandra observation, however we noted that the ASM count rate during the XTE observation was 2.46 ± 0.30 C/s, compatible with the ASM count rate during the observation discussed in this work.
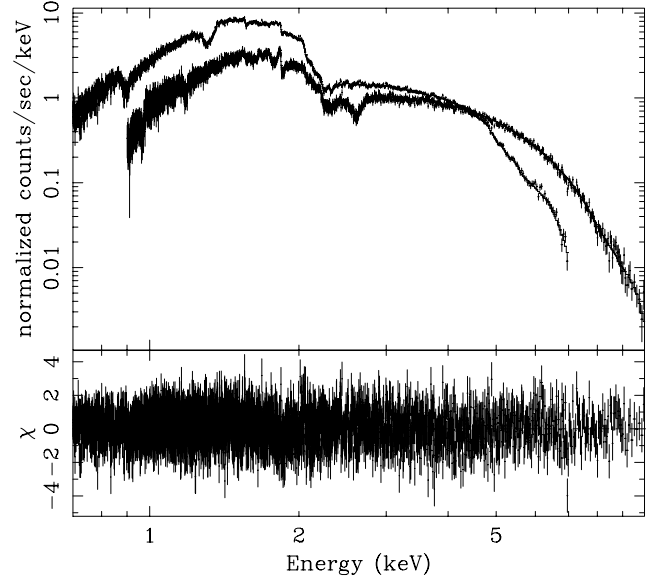
Finally we note that the best-fit values of the absorbing equivalent hydrogen column N_H of each model were smaller than 0.29×10^{22} cm^{-2}, the Galactic column density measured

Table 1. The photoelectric absorption is indicated as N_{H}. Uncertainties are at 90% confidence level for a single parameter; upper limits are at 95% confidence level. kT_{in} and k are, respectively, the accretion disk temperature and normalization in units of $R_{\mathrm{in}}^2/D_{10}^2\cos\theta$, where R_{in} is the inner radius of the accretion disk in km and D_{10} is the distance in units of 10 kpc. kT_{BB} and N_{BB} are, respectively, the blackbody temperature and normalization in units of L_{39}/D_{10}^2, where L_{39} is the luminosity in units of 10^{39} erg s^{-1}; kT_{e}, τ, and N_{CompST} indicate the electron temperature, the optical depth, and the normalization of the CompST model of the Comptonizing cloud around the neutron star, respectively; N_{po} and N_{po} cutoff indicate the normalization of the power law and the cutoff power law, in unit of photons keV^{-1} s^{-1} cm^{-2} at 1 keV. E_{edge} and τ_{edge} indicate the threshold energy and the optical depth associated to the absorption edge.
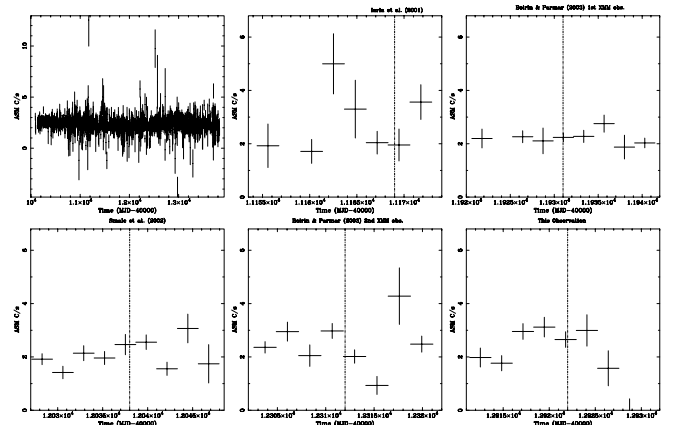
	MCD + power law	MCD + CompST	Blackbody + Power Law Cutoff
Parameters			
N_{H} ($\times 10^{22}$ cm^{-2})	$0.240^{+0.013}_{-0.017}$	$0.199^{+0.023}_{-0.010}$	$0.175^{+0.014}_{-0.016}$
E_{edge} (keV)	–	1.276 (fixed)	–
τ_{edge}	–	<0.014	–
kT_{in} (keV)	2.470 ± 0.020	0.855 (fixed)	–
k	$1.393^{+0.044}_{-0.065}$	$12.2^{+6.7}_{-5.7}$	–
kT_{BB} (keV)	–	–	$1.466^{+0.060}_{-0.115}$
N_{BB} ($\times 10^{-3}$)	–	–	$2.37^{+0.73}_{-0.87}$
photon index	$2.31^{+0.21}_{-0.20}$	–	–
N_{po}	0.0700 ± 0.0035	–	–
photon index	–	–	$1.033^{+0.069}_{-0.077}$
N_{po} cutoff	–	–	$0.1453^{+0.0040}_{-0.0047}$
E_{co} (keV)	–	–	5.9 (fixed)
kT_{e} (keV)	–	$1.759^{+0.046}_{-0.039}$	–
τ	–	$24.6^{+2.8}_{-2.0}$	–
N_{CompST}	–	$0.103^{+0.021}_{-0.023}$	–
$L_{\mathrm{0.6-10\,keV}}$ erg s^{-1}	1.2×10^{37}	1.2×10^{37}	1.2×10^{37}
χ^2(d.o.f.)	2406(2723)	2447(2722)	2412(2723)

Fig. 3. Data and residuals of the persistent emission in the energy range 0.7–10 keV for the rebinned 1st-order MEG and HEG spectra (see text). The continuum is fitted by an absorbed power law plus a MCD (Mitsuda et al. 1984) component. From the residuals is evident an absorption feature at around 7 keV.


Fig. 4. The RXTE ASM lightcurve of XB 1254–690 (*top-left panel*). In the others panels we expanded the temporal scale to clearly show the ASM count rate during the previous observations of the source. The dash-pointed vertical lines indicate the start times of the BeppoSAX observation (*top-center panel*), XMM observations (*top-right and bottom-center panels*), RXTE PCA observation (*bottom-left panel*), and this observation (*bottom-right panel*).

toward XB 1254–690 in the 21 cm radio survey of Dickey & Loekman (1990). We reported the parameters of the continuum models in Table 1, since the three adopted models gave similar residuals we adopted the continuum model composed of MCD plus power law in the following of this section. In the next section we briefly discussed the three models. We reported the data and the residuals in Fig. 3 and the ASM lightcurve of XB 1254–690 in Fig. 4.

From an accurate analysis of the residuals we detected two absorption features between 0.8 and 0.9 keV, and an absorption feature near 7 keV, their presence was model independent. To resolve the absorption features we fixed the continuum and added a Gaussian line with negative normalization for each feature. We used the 1st-order MEG spectrum to resolve the absorption features below 1 keV and the 1st-order HEG spectrum to resolve that near 7 keV. The absorption features below 1 keV were centered at 0.835 and 0.849 keV with a significance of 3σ and 2.4σ, and equivalent widths of -0.65, and -0.69 eV, respectively. Since these lines have a low significance and a no clear identification we retained that they could be due to statistical fluctuations in the MEG instrument (see the Discussion). In the 6–8 keV energy range we detected an absorption line centered at 6.962 keV with a significance of 3.7σ, corresponding to Fe XXVI K$_\alpha$; the equivalent width was -15.8 eV. In Fig. 5 we showed the residuals with respect to the continuum in the

6–8 keV energy range, in Table 2 we reported the best-fit parameters of the three observed absorption lines.

4. Discussion

We have analyzed a 53 ks Chandra observation of the persistent emission from XB 1254–690. The position of the zeroth-order image of the source provides improved X-ray coordinates for XB 1254–690 (RA = 12$^{\mathrm{h}}$57$^{\mathrm{m}}$37$^{\mathrm{s}}$.153, Dec = $-69°17'18''.98$), with an angular separation of 2$''$ to the X-ray position reported by the "Coordinate Converter" tool (see Sect. 2), impossible to distinguish from the analysis of the two previous XMM observations (Boirin & Parmar 2003) because the larger spatial resolution of all the XMM EPIC cameras. We performed a spectral analysis of the persistent emission using the
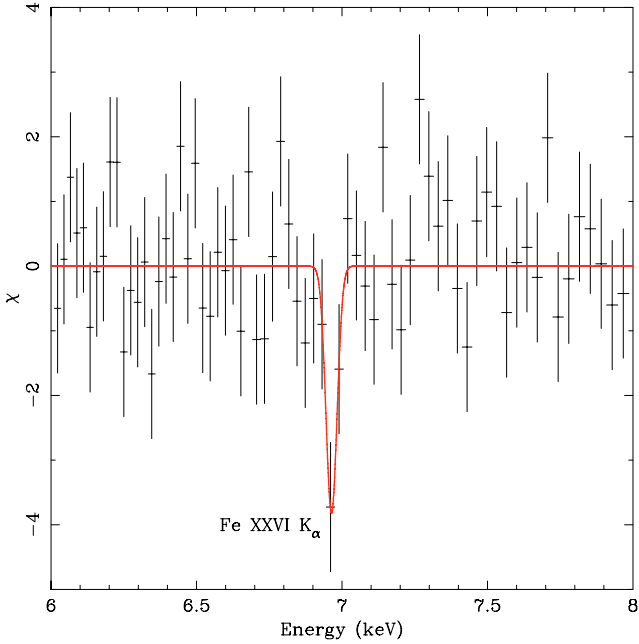
Fig. 5. Residuals with respect to the best-fit model of the continuum reported in Table 2 of the 1st-order HEG spectrum. In the panel the residuals are plotted in the energy intervals around the Fe XXVI absorption line.

1st-order MEG and HEG spectra. The continuum emission was well fitted by three different models: a MCD component plus a power law, a MCD component plus a Comptonized component (CompST in XSPEC), and a blackbody plus a power law with cutoff. We obtained from these models an unabsorbed luminosity of 1.2×10^{37} erg s^{-1} in the 0.6–10 keV energy range. The first model was the same adopted by Boirin & Parmar (2003) to fit the XMM spectra of XB 1254–690 giving similar best-fit parameters, the second model was the same adopted by Iaria et al. (2001) in the 0.6–10 keV energy range using BeppoSAX data finding, again, similar best-fit parameters, and, finally, the third model was the same adopted by Smale et al. (2002) using RXTE PCA data and also in this case we obtained comparable best-fit values. The statistically equivalence of the three models suggested that the state of the XB 1254–690 was stable during the observations from 1998 December (date of the BeppoSAX observation) up to 2003 October (date of this observation). This conclusion was also suggested by our analysis of the ASM lightcurve that showed a similar value of the count rate during the four observations.

We noted that the model composed of a MCD component plus a power law appeared not physically plausible, since it was hard to explain the small inner radius associated to the best-fit parameters of the MCD component. In fact, the inner radius associated to the temperature of 2.47 keV was $R_{\rm in} \sqrt{\cos\theta} \simeq 1.2$ km and taking into account the inclination angle θ of XB 1254–690, that is between 65° and 73° (Courvoisier et al. 1986; Motch et al. 1987), we found $R_{\rm in} \simeq 2$ km, much less than the neutron star radius. On the other hand the model composed of a MCD component plus a Comptonized component, already discussed by Iaria et al. (2001), implied that the inner radius of the accretion disk was between 5 and 6 km. Since the electron scattering could modify the MCD emission (Shakura & Sunyaev 1973; White et al. 1988), we corrected the value of the inner radius and its temperature for this effect obtaining $R_{\rm in} \simeq 17$ km (see Iaria et al. 2001 and references therein for a more detailed

discussion). The Comptonized component could be associated to a corona having a temperature of 2 keV and surrounding the neutron star, as proposed by the Eastern Model (Mitsuda et al. 1989). Finally, the model composed of a power law with energy cutoff plus a blackbody component was consistent to the Birmingham Model (see Church & Balucinska-Church 2004). In this case the blackbody emission is thermalized emission from the neutron star and the cutoff power-law emission is produced in an extended corona above the accretion disk. Unfortunately the narrow 0.7–10 keV energy range could not allow us to discriminate between these models although the scenario proposed by the Birmingham model better described the line widths found in our analysis (see below).

At high energies we detected a Fe XXVI K$_\alpha$ absorption line. The Fe XXVI absorption line was already observed by Boirin & Parmar (2003) using two XMM EPIC pn observations, in that case an upper limit of 95 eV was estimated on the line width. Thanks to the higher spectral resolution of Chandra HEG and to an observation four times longer, we found that the corresponding line width was <35 eV. Furthermore, Boirin & Parmar (2003) detected a weak absorption feature at 8.16 ± 0.06 keV proposing two possible interpretations of it: a) an absorption line associated to Fe XXVI K$_\beta$, although the centroid should have to be 8.26 keV and then not compatible to the best-fit value reported by them, and b) a systematic feature due to the uncertain calibration of the EPIC pn, in that spectral region, at the time of their analysis. We did not detect any absorption feature which could be associated to Fe XXVI K$_\beta$ but we could not exclude that the low effective area of the 1st-order HEG above 7 keV did not allow us to detect it. To check this possibility we added a Gaussian absorption line with the centroid and the line width fixed to 8.16 keV and 10 eV, respectively. We found an upper limit of the equivalent width >−15 eV that was compatible to that obtained from the XMM observations, then we could not discriminate between the two possible explanations about the origin of this narrow feature given by Boirin & Parmar (2003).

Since we observed only the Fe XXVI K$_\alpha$ and did not have evidence of a Fe XXV absorption lines we deduced that the ionization parameter associated to this line was $\log(\xi) > 4$ erg cm s^{-1}. We found the upper limit to the equivalent width associated to the Fe XXV absorption line fixing its centroid and its line width to 6.7002 keV and 10 eV, respectively, and finding a value >−2.6 eV. We estimated the Fe XXV and Fe XXVI column densities using the relation:

$$\frac{W_\lambda}{\lambda} = \frac{\pi e^2}{m_{\rm e} c^2} N_j \lambda f_{ij} = 8.85 \times 10^{-13} N_j \lambda f_{ij}$$

where N_j is the column density for the relevant species, f_{ij} is the oscillator strength, W_λ is the equivalent width of the line, and λ is the wavelength in centimeters (Spitzer 1978, p. 52). Adopting $f_{ij} = 0.798$ and $f_{ij} = 0.416$ for Fe XXV and Fe XXVI respectively (see Verner & Yakovlev 1995), and the best parameters reported in Table 2, we found $N_{\rm FeXXV} \lesssim 1.1 \times 10^{17}$ cm^{-2} and $N_{\rm FeXXVI} \simeq 3.5 \times 10^{17}$ cm^{-2}. We noted that these values were similar to those estimated by Lee et al. (2002) for GRS 1915+105 where the ionization parameter was estimated by the authors to be $\log(\xi) > 4.15$ erg cm s^{-1}. A further confirm about the goodness of our estimation of ξ could be obtained considering the Chandra spectroscopic results of the dipping source XB 1916–053 (Iaria et al. 2006) which had an unabsorbed luminosity of 7.5×10^{35} erg s^{-1} in the 0.6–10 keV energy range. In that case, assuming an ionization continuum consisting of a power law with $\Gamma = 2$ (Kallman & Bautista 2001), the ionization parameter had been estimated to be $\log(\xi) \simeq 4.15$ erg cm s^{-1} from the observed Fe XXV and

Table 2. The parameters of the Gaussian absorption lines are E, σ, I, EW, and $FWHM$ indicating the centroid, the width, the intensity in units of photons s^{-1} cm^{-2}, the equivalent width, and the Full Width Half Maximum of the lines, respectively.

	Parmeters
E (keV)	$0.83505^{+0.00051}_{-0.00055}$
σ (eV)	<1.2
I ($\times 10^{-4}$ cm^{-2} s^{-1})	$-1.11^{+0.57}_{-0.83}$
EW (eV)	$-0.65^{+0.33}_{-0.48}$
$FWHM$ (km s^{-1})	<1020
E (keV)	$0.8486^{+0.0027}_{-0.0014}$
σ (eV)	$1.00^{+4.09}_{-0.73}$
I ($\times 10^{-4}$ cm^{-2} s^{-1})	$-1.16^{+0.76}_{-1.60}$
EW (eV)	$-0.69^{+0.45}_{-0.95}$
$FWHM$ (km s^{-1})	830^{+3400}_{-670}
Fe XXVI K$_\alpha$	
E (keV)	$6.962^{+0.012}_{-0.015}$
σ (eV)	<35
I ($\times 10^{-4}$ cm^{-2} s^{-1})	$-1.22^{+0.52}_{-0.66}$
EW (eV)	$-15.8^{+6.7}_{-8.5}$
$FWHM$ (km s^{-1})	<3550

Fe XXVI absorption lines. Since in this case we did not detect the Fe XXV absorption line we suggested that the ionization parameter associated to the Fe XXVI absorption line was larger than $10^{4.15}$ erg cm s^{-1}. Furthermore we were confident of our result because Diaz Trigo et al. (2005) obtained a similar value of the ionization parameter ($\log(\xi) = 4.3 \pm 0.1$ erg cm s^{-1}) analysing the same XMM data of XB 1254–690 presented above. Finally we noted that the temperature associated to a photoionized plasma having a ionization parameter $\log(\xi) > 4.15$ erg cm s^{-1} should be $T \gtrsim 2.4 \times 10^6$ K (see Lee et al. 2002; Kallman & Bautista 2001).

At low energies we detected two weak absorption lines at 0.835 and 0.849 keV, respectively. Using the rest frame wavelengths reported by Verner et al. (1996) we noted that no lines are associated to 0.835 keV, on the other hand the line at 0.849 keV could be associated to Fe XVIII and/or Fe XIX but in this case we should observe more prominent absorption lines associated to these ions that were not observed, for this reason we retained that probably the presence of these features in the spectra was due to statistical fluctuations taking also in account their low statistical significance.

Boirin & Parmar (2003) found a soft excess in the EPIC pn spectra, they tried to fit it using an absorption edge at 1.27 keV as reported by Iaria et al. (2001), however the larger spectral resolution of the EPIC pn indicated that a Gaussian emission line centered at 0.93 keV with a corresponding equivalent width of ~30 eV and a width ~175 eV improved the fit below 2 keV. Boirin & Parmar (2003) discussed that the nature of the emission feature was uncertain and its presence in the EPIC pn spectra was almost model independent. We investigated this feature adding an absorption edge with the threshold energy fixed to the value reported by Iaria et al. (2001) and finding an upper limit of 0.014 associated to the optical depth, this value was not compatible to 0.154 ± 0.059 obtained by Iaria et al. (2001). Moreover we noted that the soft excess observed in the EPIC pn spectra by Boirin & Parmar (2003) was not present in our residuals (see Fig. 3). It is worth to note that a similar soft excess was also observed in the EPIC pn spectrum of the dipping source 4U 1323–62 by Boirin et al. (2005), in that case the

simultaneous RGS spectrum did not show the soft excess and the authors discussed the broad emission feature as a probable instrumental artifact. This conclusion could be valid also for the XMM observation of XB 1254–690 although the lack of a simultaneous XMM RGS spectrum could not give a clear confirm of our idea.

We investigated the nature of the Fe XXVI line width. A plausible scenario, already adopted to describe the line width of the absorption lines present in the Chandra spectrum of the dipping source XB 1916–053 (Iaria et al. 2006), is that the line was broadened by some bulk motion or supersonic turbulence with a velocity below 1000 km s^{-1} as indicated by the FWHMs of the lines (see Table 2). Assuming that the mechanism generating the turbulence or bulk motion was due to the presence of the extended corona we can achieve some informations about where the Fe XXVI absorption line was produced. Coronal models tend to have turbulent velocities which are locally proportional to the virial or rotational velocity (Woods et al. 1996). At ~8×10^9 cm (the coronal radius, see Church & Balucinska-Church 2004) the virial velocity should be 1500 km s^{-1}, considering a neutron star of 1.4 $M_\odot$. This velocity was similar to the values obtained from the FWHM of the Fe XXVI absorption line suggesting that it could be produced between the coronal radius and the disk edge (~4×10^{10} cm, see Church & Balucinska-Church 2004).

5. Conclusion

We studied the persistent emission of XB 1254–690 using a 53 ks Chandra observation. We improved the position of the source, the new coordinates are RA = $12^h57^m37\overset{s}{.}153$, Dec = $-69°17'18\overset{''}{.}98$ (J2000.0) with an uncertainty circle of the absolute position of $0.6''$.

We confirmed the presence of the Fe XXVI Ly$_\alpha$ absorption lines at 6.962 keV already observed by XMM-Newton. Since a Fe XXV absorption line was not observed we estimated that the ionization parameter $\log(\xi)$ was larger than 4.15 erg cm s^{-1}.

The unabsorbed luminosity in the 0.6–10 keV energy range, 1.2×10^{37} erg s^{-1}, similar to the values obtained from the previous BeppoSAX (Iaria et al. 2001) and XMM (Boirin & Parmar 2003) observations. We estimated that the width of the Fe XXVI absorption line could be compatible with a broadening caused by bulk motion or turbulence connected to the coronal activity, finding from the broadening that it was produced at a distance from the neutron star between the coronal radius (8×10^9 cm) and the disk edge (4×10^{10} cm).

References

Boirin, L., & Parmar, A. N. 2003, A&A, 407, 1079
Boirin, L., Parmar, A. N., Barret, D., Paltani, S., & Grindlay, J. E. 2004, A&A, 418, 1061
Boirin, L., Mendez, M., Diaz Trigo, M., et al. 2005, A&A, 436, 195
Church, M. J., & Balucinska-Church, M. 2004, MNRAS, 348, 955
Courvoisier, T. J.-L., Parmar, A. N., & Peacock, A. 1984, IAU Circ., No 3952
Courvoisier, T. J.-L., Parmar, A. N., Peacock, A., & Pakull, M. 1986, ApJ, 309, 265
Davis, J. E. 2001, ApJ, 562, 575
Diaz Trigo, M., Parmar, A. N., Boirin, L., et al. 2005, [arXiv:astro-ph/0509342]

Dickey, J. M., & Loekman, F. J. 1990, ARA&A, 28, 215

Garmire, G. P., Bautz, M. W., Ford, P. G., Nousek, J. A., & Ricker, G. R. Jr. 2003, Proc. SPIE, 4851, 28

Griffiths, R. E., Gursky, H., Schwartz, D. A., et al. 1978, Nature, 276, 247

Iaria, R., Di Salvo, T., Burderi, L., & Robba, N. R. 2001, ApJ, 548, 883

Iaria, R., Di Salvo, T., Lavagetto G., Robba, N. R., & Burderi, L. 2006, [arXiv:astro-ph/0605055]

Juett, A. M., & Chakrabarty, D. 2006, [arXiv:astro-ph/0604046]

Kallman, T., & Bautista, M. 2001, ApJS, 133, 221

Kotani, T., Ebisawa, K., Dotani, T., et al. 2000, ApJ, 539, 413

Lewin, W. H. G., & Joss, P. C. 1983, in Accretion Driven Xηray Stellar Sources, ed. W. Lewin, & E. van den Heuvel (Cambridge: Cambridge University Press), 41

Mason, K. O., Middleditch, J., Nelson, J. E., & White, N. E. 1980, Nature, 287, 516

Miller, J. M., Fabian, A. C., Wjinands, R., et al. 2002, 578, 348

Miller, J. M., Raymond, J., Homan, J., et al. 2004, [arXiv:astro-ph/0406272]

Mitsuda, K., Inoue, H., Koyama, K., et al. 1984, PASJ, 36, 741

Mitsuda, K., Inoue, H., Makamura, N., & Tanaka, Y. 1989, PASJ, 41, 97

Motch, C., Pedersen, H., Beuermann, H., Pakull, M. W., & Courvoisier, T. J.-L. 1987, ApJ, 313, 792

Shakura, N. I., & Sunyaev, R. A. 1973, A&A, 24, 337

Smale, A. P., & Wachter, S. 1999, ApJ, 527, 341

Smale, A. P., Church, M. J., & Balucinska-Church, M. 2002, ApJ, 581, 1286

Spitzer, L. 1978, Physical Processes in the Interstellar Medium (New York: Wiley)

Ueda, Y., Inoue, H., Tanaka, Y., et al. 1998, ApJ, 492, 782

Ueda, Y., Murakami, H., Yamaoka, K., et al. 2004, ApJ, 609, 325

Uno, S., Mitsuda, K., Aoki, T., & Makino, F. 1997, PASJ, 49, 35

Verner, D. A., & Yakovlev, D. G. 1995, A&AS, 109, 125

Verner, D. A., Verner, E. M., & Ferland, G. J. 1996, At. Data Nucl. Data Tables, 64, 1

White, N. E., Stella, L., & Parmar, A. N. 1988, ApJ, 324, 36

Woods, D. T., Klein, R. I., Castor, J. I., et al. 1996, ApJ, 461, 767

Yamaoka, K., Ueda, Y., Inoue, H., et al. 2001, PASJ, 53, 179